ARTICLE IN PRESS

ELSEVIER

Physica E ▮▮▮ (▮▮▮▮) ▮▮▮–▮▮▮

PHYSICA E

www.elsevier.com/locate/physe

Marvellous things in marvellous rings: energy spectrum, spins and persistent currents

T. Ihn[a,*], A. Fuhrer[a], T. Heinzel[a], K. Ensslin[a], W. Wegscheider[b,c], M. Bichler[c]

[a] *Solid State Physics Laboratory, ETH Zürich, 8093 Zürich, Switzerland*
[b] *Angew. und Expt. Physik, Universität Regensburg, 93040 Regensburg, Germany*
[c] *Walter Schottky Institut, Technische Universität München, 85748 Garching, Germany*

Abstract

Magnetotransport experiments on a semiconductor quantum ring in the Coulomb blockade regime are described. The measurements allow to extract the discrete energy levels of a realistic ring, which are found to agree well with theoretical expectations. The interaction effects important for our ring structure are analysed in detail. The experimentally observed charging energy can be quantitatively understood within the Hartree approximation including a strong screening contribution due to the top gate. The strong screening effect is the reason for the frequent occurrence of spin-pairs in the addition spectra. The relation of the observed addition spectra to persistent currents is established and the magnitude of the current is extracted from experimental data.

PACS: 73.23.Hk; 73.21.La; 73.23.Ra; 73.63.Kv

Keywords: Quantum dots; Coulomb-blockade; Aharonov–Bohm effect; Persistent currents; Spin-pairing

1. Introduction

Ring structures have become especially important for mesoscopic physics in connection with the Aharonov–Bohm effect [1] and related phenomena [2]. On the experimental side, the Aharonov–Bohm effect has been observed in metal rings [3,4] and in semiconducting rings [5,6]. Recently, the phase coherence of transport through a quantum dot embedded in one arm of an open ring has been demonstrated [7,8]. Persistent currents [9] were experimentally detected by measuring the magnetic response of 10^7 mesoscopic copper rings [10] and in a single isolated gold loop [11]. The only measurements of persistent currents in a GaAs/AlGaAs heterostructure are due to Mailly et al. [12]. The energy spectrum of self-assembled closed rings has recently been analysed by optical experiments [13,14].

The quantum ring samples for our experiments have been fabricated on AlGaAs/GaAs heterostructures containing a two-dimensional electron gas (2DEG) with density 5×10^{11} cm^{-2} and mobility 90 m^2/V s at $T = 4.2$ K only 34 nm below the sample surface. The surface of the heterostructure has been locally oxidized by applying a voltage between the conductive tip of an atomic force microscope (AFM) and the 2DEG [15,16]. The electron gas is depleted below the oxidized regions, which was used in other studies for defining high-quality quantum dots [17]. Fig. 1(a) shows an AFM image of the oxide lines defining the quantum ring. The width of the

* Corresponding author.
E-mail address: ihn@phys.ethz.ch (T. Ihn).

1386-9477/02/$ - see front matter © 2002 Published by Elsevier Science B.V.
PII: S1386-9477(02)00592-1

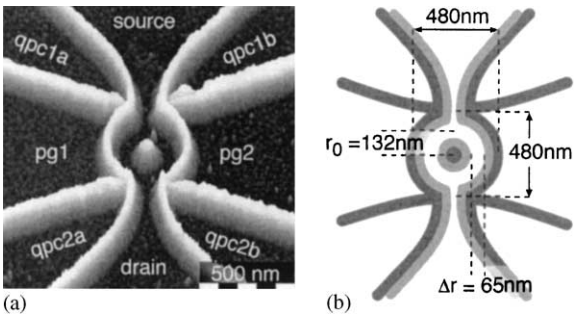

Fig. 1. Sample layout. (a) AFM image of the quantum ring taken after writing the structure. The oxide lines (bright regions) separate the sample into several conductive (dark) regions. (b) Schematic sketch of the ring. The dark curves represent the oxide lines. We estimate the depletion length to be about 50 nm which results in an estimated channel width of $\Delta r \approx 65$ nm. The average radius of the ring is $r_0 = 132$ nm.

quantum point contacts connecting the ring to source (drain) is controlled by voltages applied to the lateral gate electrodes qpc1a and b (qpc2a and b). The number of electrons in the ring can be tuned via the lateral plunger gates pg1 and 2. Shape deformations due to applied in-plane gate voltages are known to be relatively weak [16,17]. The schematic in Fig. 1(b) shows the dimensions of the quantum ring. After the oxidation step the sample has been covered with a metallic top gate electrode. We will show below that with the combination of in-plane and top gate electrodes the quantum ring can be tuned into the Coulomb blockade regime with the single-particle level spacing being much larger than the thermal energy kT.

An upper limit for the number of radial subbands in the dot can be estimated from the width $\Delta r \approx 65$ nm of the ring and the Fermi-wavelength of the electrons in the host material $\lambda_F \approx 35$ nm to be 3–4. However, it is known that the electron density in strongly confined quantum dots can be much smaller than the two-dimensional electron density of the host material and λ_F can be much larger. This means that the number of radial modes is very likely to be smaller than 3 and we estimate the number of electrons in the ring to be less than 200.

2. Energy spectra of quantum rings

Fig. 2(b) presents a logarithmic greyscale plot of the current through the quantum ring as a function of a voltage applied to both plunger-gates and magnetic field B (applied normal to the 2DEG plane). A constant DC source-drain voltage $V_{SD} = 20$ μV was applied at a temperature of 100 mK in a dilution refrigerator.

In Fig. 2(a) the Coulomb-blockade oscillations have been extracted along the horizontal dashed line in Fig. 2(b), i.e. at constant $B = 92$ mT. A series of current peaks can be seen that vary strongly in height from peak to peak. The highest peaks correspond to a conductance of a few percent of the conductance quantum e^2/h. The full-width at half-maximum of most peaks is of the order of $4kT$ (with $T = 100$ mK) indicating thermal broadening of conductance resonances. In between the peaks the current is typically unmeasurably small. All these observations indicate that the ring is in the Coulomb blockade regime.

Extracting the conductance as a function of magnetic field along the dashed vertical line of constant gate voltage leads to the trace in Fig. 2(c). It shows oscillatory behaviour with a period of $\Delta B = 75$ mT, i.e. one flux quantum h/e per area πr_0^2. This is exactly the Aharonov–Bohm period of an open ring of the same radius. It can be seen that the positions and amplitudes of most peaks in Fig. 2(b) show this period as well. This is the manifestation of Aharonov–Bohm-type effects in the quantum ring.

The greyscale plot in Fig. 2(d) shows the conductance of the ring in the V_{SD}-V_{tg}-plane measured at zero magnetic field. Typical Coulomb-blockade diamonds are observed separated by the conductance peaks at $V_{SD} = 0$. At larger V_{SD} outside the white Coulomb-blockade diamonds, conductance peaks of excited dot states can be seen.

In the following we interpret our data using the constant interaction model of the Coulomb-blockade effect [18,19]. From measurements of the Coulomb-blockade diamonds [for a typical example see Fig. 2(d)] in the V_{SD}–V_{tg} plane and in the V_{SD}–V_{pg} plane we determine the lever arms of the top- and in-plane gates allowing us to translate gate voltages into energies, and the charging energy $E_c = e^2/C_\Sigma \approx 190$ μeV which is much larger than $kT \approx 10$ μeV. The observed single-particle level spacings obtained from the conductance peak separations after subtraction of E_c are found to be as large as $\Delta \approx 180$ μeV (see below). This value agrees with the large separation of excited states from the Coulomb-blockade diamond boundaries in Fig. 2(d). We emphasize that such a large single-level

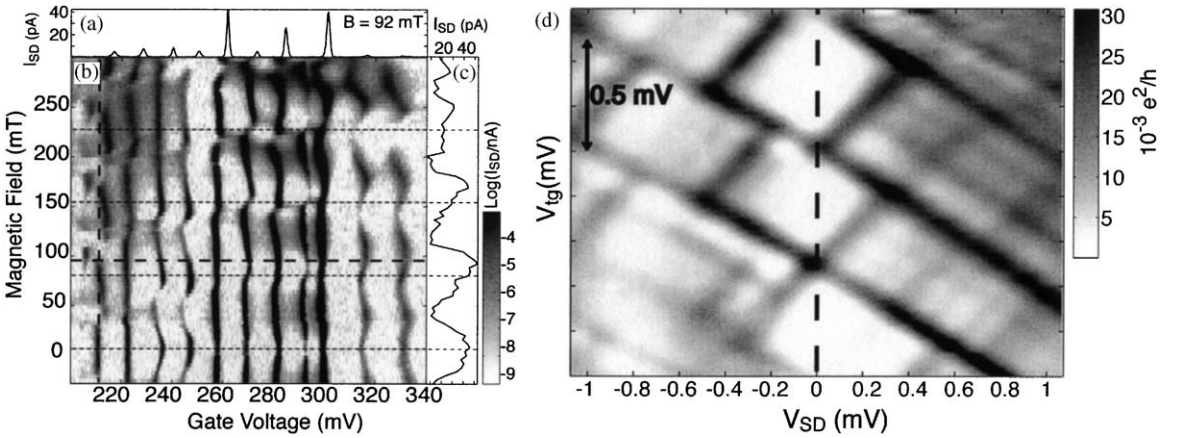

Fig. 2. The addition spectrum. (a) Measurement of Coulomb blockade resonances at fixed magnetic field. (b) The evolution of such sweeps with magnetic field results in the addition spectrum shown in colour. The Aharonov–Bohm period expected from the ring geometry is indicated by the thin white horizontal lines. (c) Magnetic field sweep for constant gate voltage $V_{pg} = 218$ mV (dashed line in the colour plot). (d) Typical Coulomb-blockade diamonds measured at zero magnetic field.

spacing is usually not achieved for quantum dots of comparable size. In the ring it is due to the exclusion of electrons from the central region accomplished by the presence of the antidot. Since $\Delta \gg kT$ we can state that we are in the single-level transport regime if we neglect occasional level degeneracies. Within the constant interaction model the positions of the Coulomb-blockade peaks in gate voltage are given by

$$U_G^{(N)}(B) = \frac{1}{e\alpha_G}\left[\varepsilon_N(B) + E_c\left(N - \frac{1}{2}\right) - \mu_S\right]. \quad (1)$$

Here we have assumed that the lever arm α_G, the charging energy E_c and μ_S, the electrochemical potential in source and drain contacts, are independent of magnetic field. This assumption is reasonable at small magnetic fields where the orbital wave functions in the ring are not significantly changed compared to $B=0$. Under this assumption the magnetic field dispersion of individual conductance peaks in the measured addition spectrum in Fig. 2(b) directly reflects the dispersion of individual single-particle levels.

The experimental conductance-peak positions are obtained from measurements like the ones shown in Fig. 2(b) by converting the gate-voltage axis into an energy scale using the lever arm determined from Coulomb-blockade diamonds [20] and subtracting a constant charging energy of 190 μeV. The resulting energies are plotted in Fig. 3 as a function of

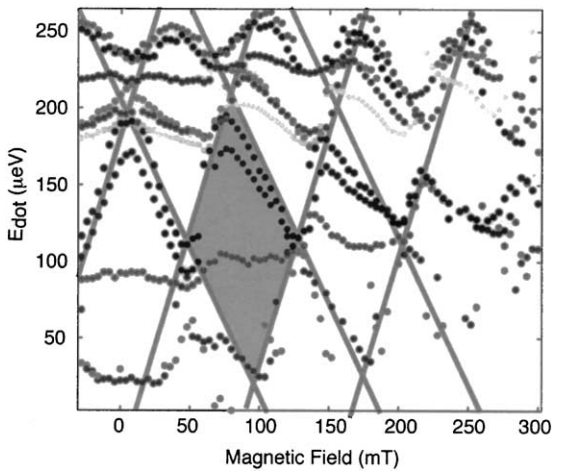

Fig. 3. Reconstruction of the energy spectrum of the ring from the data shown in Fig. 2. The straight grey lines show the diamond-like pattern expected from an ideal ring spectrum.

magnetic field. The orbital states move up and down in magnetic field with the Aharonov–Bohm period ΔB. Diamond-like patterns can be identified which are characteristic for ring spectra [21]. In this respect our experiments show the long-predicted energy spectrum characteristic for quantum rings [2,22,23]. However, the experimental spectrum shows features that are not found in the spectra of ideal rings. For example, there

are some states having a very weak magnetic field dispersion. All the features of this ring spectrum can be interpreted using a model with a small additional potential, breaking the perfect circular symmetry of the ring [21], which will always be present in the experiment due to the presence of source and drain contacts and residual disorder in the ring.

3. Interaction effects and spin-pairing

We continue with a discussion of interaction effects in our ring. A quite general treatment of the electrostatics of quantum dots in the Hartree-approximation has been given by Hallam and co-workers [24]. The Hartree energy contribution for the addition of an electron in state $\varphi_i(\mathbf{r})$ to an N-electron system is given by [25,26]

$$E_{\mathrm{H}} = e\int \mathrm{d}^3 r |\varphi_i(\mathbf{r})|^2 V_{\mathrm{H}}(\mathbf{r}) \quad \text{with}$$

$$V_{\mathrm{H}}(\mathbf{r}) := \int \mathrm{d}^3 r' \rho(\mathbf{r}') G(\mathbf{r},\mathbf{r}').$$

Here $\rho(\mathbf{r})$ is the charge density due to the N electrons already residing on the dot and the Green's function $G(\mathbf{r},\mathbf{r}')$ is the electrostatic potential at $\mathbf{r}$ created by a unit charge at position $\mathbf{r}'$. For our purposes we include the image charge effect due to the top-gate electrode located at a distance $d \approx 40$ nm from the electron gas. In general, it is not possible to calculate the Hartree energy analytically for arbitrary wave functions. Usually, a three-dimensional numerical self-consistent calculation is necessary for this purpose [27]. Here we restrict ourselves to a simplified scheme for calculating the Hartree energy. We assume that the N electrons on the dot create a homogeneous strictly two-dimensional electron density around the ring located between the inner radius r_1 and the outer radius r_2. We further assume that the electron to be added goes into a state that can be approximated by a similar homogeneous probability density distribution. For this simplified case we were able to evaluate the Hartree energy analytically. Fig. 4 shows a comparison of the calculated charging energies with and without the screening effect of the top gate. It can be seen that the presence of the top gate reduces the charging energy to about 40% of its unscreened value. In the ring structure measured in these experiments, the ratio

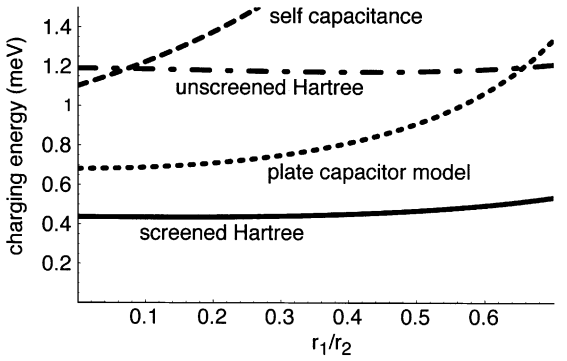

Fig. 4. Quenching of the charging energy due to screening of the Hartree contribution of the interaction by the top-gate electrode with a separation d from the ring. The ring has an inner (outer) diameter of r_1 (r_2). A value of $2d/r_2 = 0.486$ was used for this calculation. The ratio $r_1/r_2 \approx 0.6$ in our experiment. The dash–dotted curve is the result of the Hartree calculation without the screening effect, while the full curve contains screening by the top gate. For comparison we show the charging energies obtained from the constant interaction model using a self-capacitance model (dashed) and a plate capacitor model (dotted).

$r_1/r_2 \approx 0.6$. From the figure we read a charging energy of 500 μeV for this value. This charging energy does not correspond to the measured total charging energy of the dot, e^2/C_Σ, because C_Σ is the sum of many capacitances between dot and gate electrodes. The dot top-gate capacitance $C_{\mathrm{tg}} < C_\Sigma$ is only one of these contributions. From the experiment, using the lever arm of the top gate $\alpha_{\mathrm{tg}} = C_{\mathrm{tg}}/C_\Sigma$, we determine $e^2/C_{\mathrm{tg}} = 550$ μeV in nice agreement with the calculation. This quantitative result is also relevant for measurements in the Coulomb blockade regime on other quantum dots fabricated with AFM-lithography [17].

In order to check the validity of the simplest capacitive models used for estimating the charging energy, we compare to a naive model of the self-capacitance of a ring with capacitance $C_{\mathrm{ring}} = 8\varepsilon\varepsilon_0(r_2 - r_1)$ and a ring shaped plate capacitor model with $C_{\mathrm{plate}} = \varepsilon\varepsilon_0\pi(r_2^2 - r_1^2)/d$. Fig. 4 shows that the self-capacitance model strongly overestimates the charging energy of the ring. Even compared to the unscreened Hartree result this model is only good in the limit $r_1 \to 0$. The plate capacitor model does account for part of the screening effects. However, for the parameters of our dot the error of this model compared to the screened Hartree result is more than 100%.

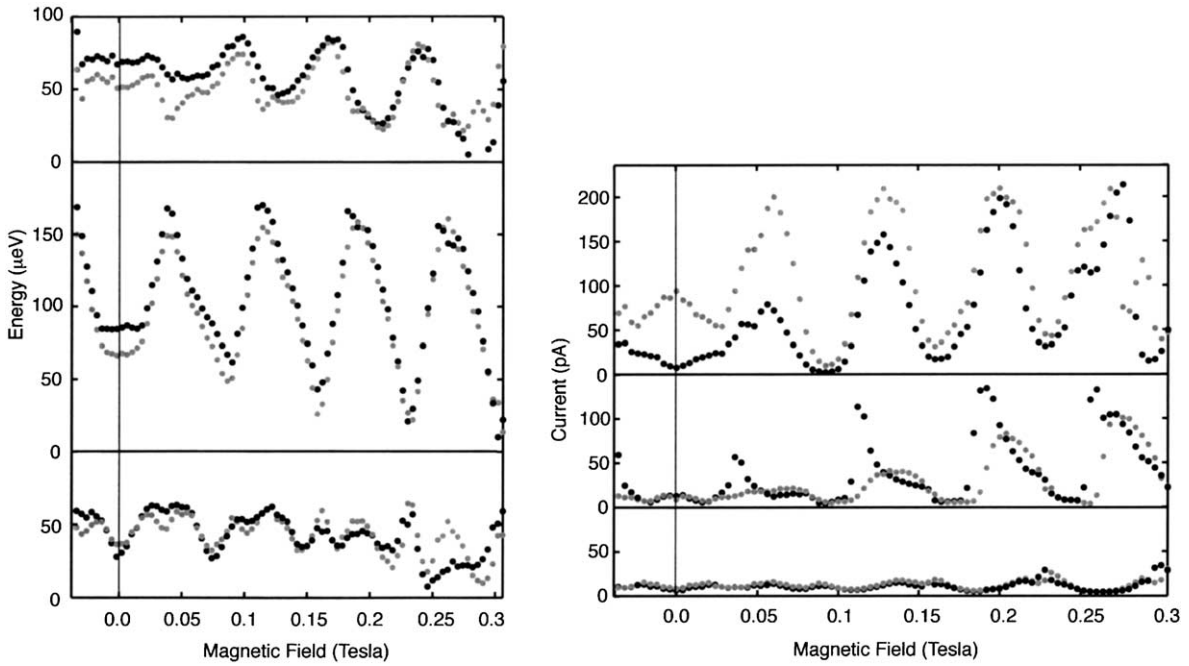

Fig. 5. Energetic position (left) and amplitude (right) of conductance peaks as a function of magnetic field for three different spin-pairs. Data for the two corresponding neighbouring conductance peaks belonging to a pair are shown in black and grey, respectively. In the graphs on the left the vertical energy axis has been obtained from the experimentally applied plunger gate voltage using the appropriate lever arm. In each pair of curves a constant charging energy of 190 μeV has been subtracted for the energetically higher peak in order to facilitate comparison. The strong correlation of energies between neighbouring peaks (left) and their respective amplitudes (right) are the signatures of spin-pairs.

The strong reduction of electron–electron interactions due to screening effects in our ring is also important for other interaction contributions such as exchange effects. It has been predicted by Blanter and co-workers [28] that subsequent occupation of the same orbital level by spin up and spin down electrons should be observed in systems with small interaction effects. In a Coulomb-blockade experiment this will show up as paired neighbouring conductance peaks with strongly correlated position and amplitude in varying magnetic field, so-called spin-pairs [17]. This is in strong contrast to the occupation of levels in real atoms or in artificial semiconductor atoms [29], where according to Hund's rules the successive filling of parallel spins is favoured. In the experiment it turns out that many spin-pairs can be observed in the quantum ring. In Fig. 5 we show three examples. On the left, the positions of conductance peaks as a function of magnetic field are shown with the charging energy subtracted. The curves of spin-pairs almost perfectly collapse onto a single curve. On the right, the corresponding amplitudes of the conductance peaks are shown. Although they are not perfectly identical for the spin-pairs, strong correlations are evident. Loosely speaking, the screening effect leads to a strong reduction of the interaction parameter r_s which is the ratio between the Coulomb interaction energy and the Fermi-energy in a two-dimensional electron gas.

4. Relation of the ring spectra to persistent currents

The existence of persistent currents in coherent mesoscopic rings was brought to the attention of the experimentalists by Büttiker and Imry [9]. We will briefly sketch the main idea below, emphasizing the relation to the single-particle energy spectrum of a

ring. The basic expression for the persistent current at zero temperature is

$$I = \frac{M}{A} = -\frac{\partial E_{\mathrm{tot}}}{\partial (B \cdot A)} = -\frac{\partial E_{\mathrm{tot}}}{\partial \Phi} = -\sum_i \frac{\partial E_i}{\partial \Phi} = \sum_i I_i.$$

Here, Φ is the total flux piercing the ring structure. The first equality stems from elementary magetostatics relating the magnetic moment M to a circulating current. The second (third) equality expresses the magnetic moment in terms of the magnetic field (flux) derivative of the total energy of the system. The total energy is then decomposed into single-particle contributions neglecting interaction effects like the charging energy. However, a charging energy independent of magnetic field can be added to E_{tot} without affecting the final result for the persistent current. We wish to emphasize that in this constant-interaction picture which is—as we have shown above—appropriate for our ring, the persistent current can be decomposed into contributions of individual single-particle levels, i.e. each state i contributes an amount to the persistent current which is given by the derivative of its energy with respect to magnetic flux.

We can now determine the contribution to the persistent current of particular states observed in the Coulomb blockade regime of our ring. For a particular strongly oscillating state in Fig. 3 we have a slope of about 300 μeV per flux quantum corresponding to $I \approx 11$ nA. States that are flattened by a symmetry breaking potential or by disorder contribute significantly less to the total persistent currents. If we assume that currents of all the lower lying states sum up to zero this current is also an estimate of the total persistent current in the ring and the determined value is consistent with previous magnetization measurements [10–12].

5. Summary

The detailed analysis of quantum rings demonstrates that even in many-electron Coulomb-blockaded systems a detailed understanding of the energy spectrum and interaction effects can be obtained. With advanced fabrication techniques at hand this opens the path to the understanding of more complex and multiply connected structures on a quantum mechanical level. Electron–electron interactions beyond the constant interaction model have been shown to play a minor role in our quantum ring leading to the frequent observation of spin-pairs. Once ring structures with only one radial mode occupied are available such quantum rings could be used to investigate spin effects [30] or even Luttinger liquid behaviour in a circular 1D system with periodic boundary conditions.

References

[1] Y. Aharonov, D. Bohm, Phys. Rev. 115 (1959) 485.
[2] A. Aronov, Y. Sharvin, Rev. Mod. Phys. 59 (1987) 755.
[3] R. Webb, S. Washburn, C. Umbach, R. Laibowitz, Phys. Rev. Lett. 54 (1985) 2696.
[4] S. Washburn, R. Webb, Adv. Phys. 35 (1986) 375.
[5] G. Timp, A. Chang, J. Cunningham, T. Chang, P. Mankiewich, R. Behringer, R. Howard, Phys. Rev. Lett. 58 (1987) 2814.
[6] A.E. Hansen, A. Kristensen, S. Pedersen, C.B.S. Rensen, P.E. Lindelof, Phys. Rev. B 64 (2001) 45327.
[7] A. Yacoby, M. Heiblum, D. Mahalu, H. Shtrikman, Phys. Rev. Lett. 74 (1995) 4047.
[8] R. Schuster, E. Buks, M. Heiblum, D. Mahalu, V. Umansky, H. Shtrikman, Nature 385 (1997) 417.
[9] M. Buttiker, Y. Imry, R. Landauer, Phys. Lett. 96 A (1983) 365.
[10] L.P. Lévy, G. Dolan, J. Dunsmuir, H. Bouchiat, Phys. Rev. Lett. 64 (1990) 2074.
[11] V. Chandrasekhar, R. Webb, M. Brady, M. Ketchen, W. Gallagher, A. Kleinsasser, Phys. Rev. Lett. 67 (1991) 3578.
[12] D. Mailly, C. Chapelier, A. Benoit, Phys. Rev. Lett. 70 (1993) 2020.
[13] A. Lorke, R. Luyken, A. Govorov, J. Kotthaus, J. Garcia, P. Petroff, Phys. Rev. Lett. 84 (2000) 2223.
[14] R. Warburton, C. Schäflein, D. Haft, F. Bickel, A. Lorke, K. Karrai, J. Garcia, W. Schoenfeld, P. Petroff, Nature 405 (2000) 926.
[15] R. Held, T. Vancura, T. Heinzel, K. Ensslin, M. Holland, W. Wegscheider, Appl. Phys. Lett. 73 (1998) 262.
[16] T. Heinzel, R. Held, S. Lüscher, K. Ensslin, W. Wegscheider, M. Bichler, Physica E 9 (2001) 84.
[17] S. Lüscher, T. Heinzel, K. Ensslin, W. Wegscheider, M. Bichler, Phys. Rev. Lett. 86 (2001) 2118.
[18] C. Beenakker, Phys. Rev. B 44 (1991) 1646.
[19] L. Kouwenhoven, C. Marcus, P. McEuen, S. Tarucha, R. Westervelt, N. Wingreen, Electron transport in quantum dots, in: L.P. Kouwenhoven, G. Schön, L. Sohn (Eds.), Nato ASI Conference Proceedings, Kluwer, Dordrecht, 1997, pp. 105–214.
[20] M. Kastner, Rev. Mod. Phys. 64 (1992) 849.
[21] A. Fuhrer, S. Lüscher, T. Ihn, T. Heinzel, K. Ensslin, W. Wegscheider, M. Bichler, Nature 413 (2001) 822.
[22] N. Byers, C. Yang, Phys. Rev. Lett. 7 (1961) 46.

[23] W.-C. Tan, J. Inkson, Semicond. Sci. Technol. 11 (1996) 1635.
[24] L. Hallam, J. Weis, P. Maksym, Phys. Rev. B 53 (1996) 1452.
[25] N.W. Ashcroft, N.D. Mermin, Solid State Physics, Saunders College Publishing, London, 1976.
[26] O. Madelung, Festkörpertheorie I: Elementare Anregungen, revised reprint Edition, Heidelberger Taschenbücher, Vol. 104, Springer, Berlin, 1988.
[27] M. Stopa, Phys. Rev. B 54 (1996) 13767.
[28] Y.M. Blanter, A. Mirlin, B. Muzykantskii, Phys. Rev. Lett. 78 (1997) 2449.
[29] S. Tarucha, D. Austing, T. Honda, R. van der Haage, L. Kouwenhoven, Phys. Rev. Lett. 77 (1996) 3613.
[30] D. Loss, P. Goldbart, Phys. Rev. B 43 (1991) 13762.